JACS
JOURNAL OF THE AMERICAN CHEMICAL SOCIETY
pubs.acs.org/JACS
Communication

Molecular-Level Control over Plasmonic Properties in Silver Nanoparticle/Self-Assembling Peptide Hybrids

Yin Wang, Xiaozhou Yang, Tianyu Liu, Zhao Li, David Leskauskas, Guoliang Liu,* and John B. Matson*

Cite This: J. Am. Chem. Soc. 2020, 142, 9158−9162
Read Online
ACCESS | Metrics & More | Article Recommendations | Supporting Information

ABSTRACT: The plasmonic properties of silver nanoparticle (AgNP) arrays are directly controlled by AgNP size, shape, and spatial arrangement. Reported here is a strategy to prepare chiral AgNP arrays templated by two constitutionally isomeric aromatic peptide amphiphiles (APAs), $\mathbf{K_SC'EK_S}$ and $\mathbf{C'EK_SK_S}$ (K_S = *S*-aroylthiooxime-modified lysine, *C′* = citrulline, and E = glutamic acid). In phosphate buffer, both APAs initially self-assembled into nanoribbons with a similar geometry. However, in the presence of silver ions and poly(sodium 4-styrenesulfonate) (PSSS), one of the nanoribbons ($\mathbf{K_SC'EK_S}$) turned into nanohelices with a regular twisting pitch, while the other ($\mathbf{C'EK_SK_S}$) remained as nanoribbons. Both were used as templates for synthesis of arrays of ∼8 nm AgNPs to understand how small changes in molecular structure affect the plasmonic properties of these chiral AgNP/APA hybrids. Both hybrids showed improved colloidal stability compared to pure AgNPs, and both showed enhanced sensitivity as surface-enhanced Raman spectroscopy (SERS) substrates for model analytes, with nanohelices showing better SERS performance compared to their nanoribbon counterparts and pure AgNPs.

Silver nanoparticles (AgNPs) are suitable substrates for catalysis,[1,2] sensing,[3,4] and antimicrobial applications,[5,6] and their properties depend heavily on their size, shape, and spatial arrangement.[7,8] Therefore, synthesis of AgNPs with well-defined dimensions and controlled spatial arrangements allows researchers to tune the properties of these materials for specific functions. Toward this end, materials including carbon nanotubes,[2] polymers,[9−11] DNA,[12,13] and peptides[14,15] have been used as scaffolds to direct the growth or assembly of AgNPs, relying on strong interactions between AgNPs or their precursors and functional groups on these scaffolds. Among these, self-assembled peptides are particularly attractive platforms for AgNP growth[16−19] because of their chemical tunability and their capacity to self-assemble into a wide variety of morphologies, including nanoribbons, nanosheets, and nanohelices, among others.[20−24] For instance, nanofibers assembled from aldehyde-functionalized peptide amphiphiles were used to template the growth of AgNPs in the presence of Tollens' solution.[16] Particularly intriguing are self-assembled peptide-based helical nanoribbons,[17] which organize achiral AgNPs into chiral assemblies. However, the structure−property relationships among the molecular composition of the template, the spatial arrangements of the AgNPs, and the resultant plasmonic properties of the hybrids remain elusive.

We recently discovered a class of constitutionally isomeric aromatic peptide amphiphiles (APAs) that self-assemble into different morphologies by changing the position of amino acid residues.[25] The key component of these APAs, each made of four amino acids, is the inclusion of two lysine residues that contain aromatic *S*-aroylthiooxime (SATO) functional groups[26] attached to their *ε*-amines.[27−31] We viewed these APAs as templates for AgNP growth, which would enable the AgNP/APA hybrids to retain the chiral imprint from the APA nanostructures. Because these APAs are constitutional isomers, we envisioned that we could control the spatial arrangements of AgNPs and therefore, the plasmonic properties of the hybrids by simply changing the order of amino acids. In this context, we report here that silver salts induce a morphological transition in two constitutionally isomeric APAs, which we used as the templates for AgNP growth. Our results showed that the APA morphology affected the spatial arrangements of AgNPs, which influenced the plasmonic properties of the hybrids, and, as a result, their sensitivity as substrates for surface-enhanced Raman spectroscopy (SERS).

We synthesized two constitutionally isomeric APAs that each contained one glutamic acid (E), one citrulline (*C′*), and two SATO-modified lysine (K_S) residues: $\mathbf{K_SC'EK_S}$ and $\mathbf{C'EK_SK_S}$ (Figures 1A−B, S1−S2). Based on our previous studies on APAs with similar structures,[25] we expected that $\mathbf{K_SC'EK_S}$ and $\mathbf{C'EK_SK_S}$ would form different self-assembled morphologies due to the different arrangements of amino acids in their structures. However, we were surprised to find that both APAs assembled into one-dimensional nanostructures with similar morphologies based on transmission electron microscopy (TEM) observations (Figure 1C and 1D). $\mathbf{K_SC'EK_S}$ formed nanoribbons with average widths of 7 ± 1 nm and lengths of a few micrometers (Figure 1C). $\mathbf{C'EK_SK_S}$ also assembled into micrometer-long nanoribbons with average widths of 6 ± 1 nm (Figure 1D). Next, we added silver nitrate ($AgNO_3$, 0.5 mM) and poly(sodium 4-styrenesulfonate)

Received: April 10, 2020
Published: May 11, 2020

https://dx.doi.org/10.1021/jacs.0c03672
J. Am. Chem. Soc. 2020, 142, 9158−9162

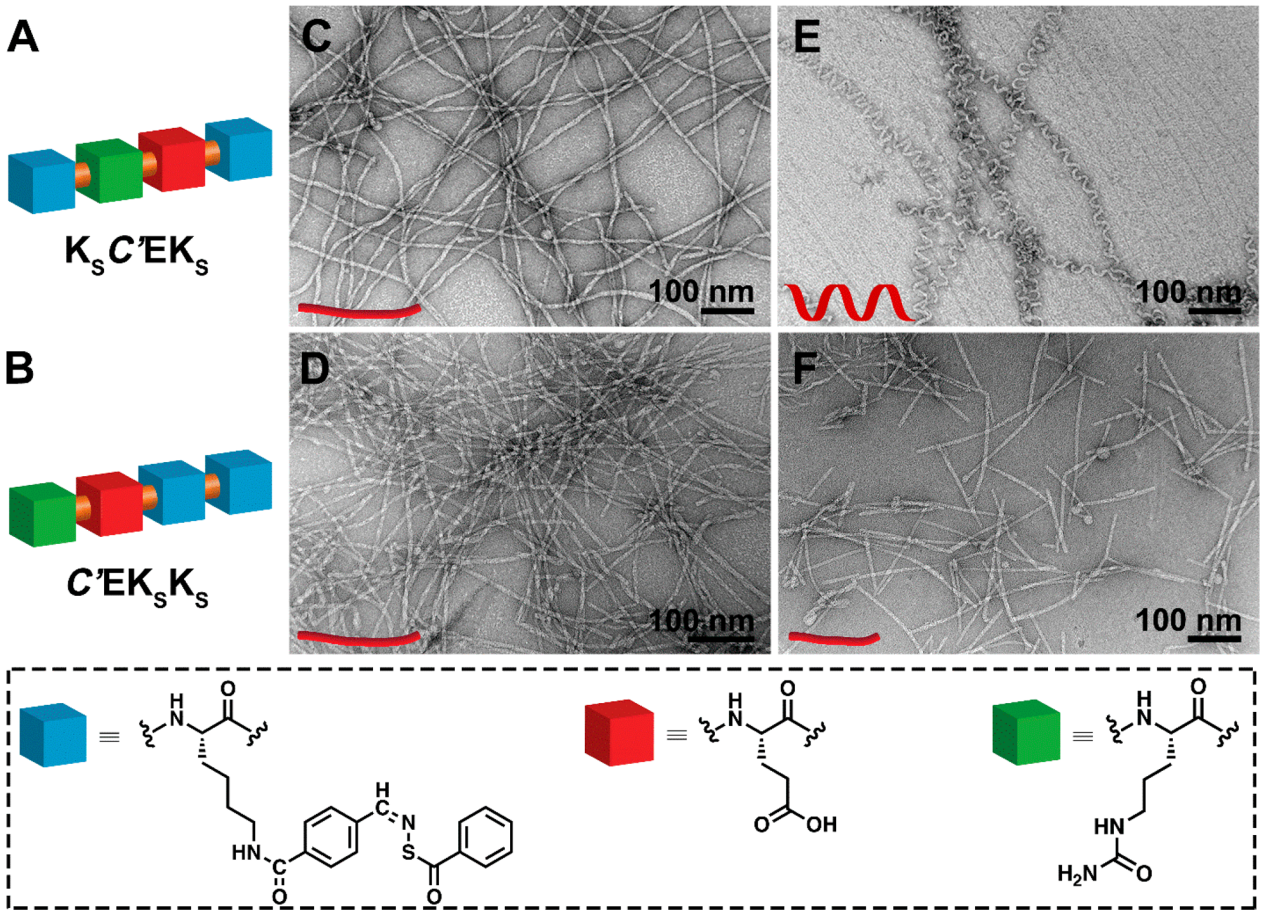

Figure 1. (A and B) Schematic illustrations of the chemical structures of the two isomeric APAs. (C–F) TEM images of (C) nanoribbons formed by $K_SC'EK_S$ and (D) $C'EK_SK_S$ in 10 mM PB; (E) nanohelices derived from $K_SC'EK_S$ and (F) short nanoribbons assembled by $C'EK_SK_S$ in 10 mM PB containing $AgNO_3$ and PSSS.

(PSSS, 0.5 mg mL^{-1}) to induce AgNP formation, which we typically use in AgNP synthesis.[32] Interestingly, upon addition of $AgNO_3$ and PSSS, the $K_SC'EK_S$ nanoribbons changed into micrometer-long nanohelices with an average diameter of 6 ± 1 nm and a regular twisting pitch of 29 ± 5 nm (Figure 1E). In sharp contrast, APA $C'EK_SK_S$ retained its nanoribbon morphology after salt addition, although the average length decreased (Figure 1F). We speculate that $K_SC'EK_S$ nanohelices form because of synergistic effects from both $AgNO_3$ and PSSS. Addition of salts could induce salting-out of APAs from solution by an excluded-volume mechanism[33] and screen the glutamic acid carboxylate groups displayed on the surface of nanoribbons, triggering a rolling up process that leads to nanohelix formation. We found that addition of only $AgNO_3$ (without PSSS) could also cause (Figure S7) but not preserve this morphological transition after AgNP growth (Figure S8). Therefore, PSSS acted as a nanohelix inducer and stabilizer during AgNP synthesis. Circular dichroism (CD) and UV–vis spectroscopy (Figures S3 and S4) were also used to examine the molecular packing before and after addition of salts (see discussion in the Supporting Information). The distinct morphology differences between $K_SC'EK_S$ and $C'EK_SK_S$ before and after salt addition exemplify how small changes in APA sequence can lead to dramatically different self-assembly behaviors, consistent with previous reports on constitutional peptide isomers.[25,34]

We next used these two nanostructured templates to synthesize AgNP/APA hybrids in a two-step process (Figure S5A). First, we added $AgNO_3$ and PSSS to a $K_SC'EK_S$ solution, followed by the reducing agent $NaBH_4$. The solution changed from colorless to yellow, suggesting the formation of small Ag seeds (AgSDs).[32] A UV–vis spectrum showed a peak near 405 nm (Figure S5B), consistent with the characteristic plasmonic response for nonaggregated, spherical AgNPs smaller than 10 nm.[35] Second, additional $AgNO_3$ solution was added dropwise into an aliquot of AgSDs (50–1000 μL) and ascorbic acid. During this second growth step, the color of the solution became bright yellow, with the peak absorption remaining at 405 nm. We determined that both a minimum amount of AgSDs and PSSS were required for maintaining the $K_SC'EK_S$ nanohelix morphology in the resultant AgNP/$K_SC'EK_S$ hybrids. Addition of too little AgSD solution resulted in the formation of nanoribbons (Figure S6), as did excluding PSSS from the synthesis (Figure S8). We then used this optimized procedure to prepare AgSDs and AgNPs templated by the $C'EK_SK_S$ nanoribbons, which showed the same color change in each step as the AgSDs and AgNPs templated by the $K_SC'EK_S$ nanohelices.

TEM was then used to examine the morphologies of the AgNP/APA hybrids and measure the sizes of the AgSDs and AgNPs in both samples. The growth of AgSDs and AgNPs had little influence on the original morphologies of these two different self-assembled APAs (Figures 2A–D). In the

https://dx.doi.org/10.1021/jacs.0c03672
J. Am. Chem. Soc. 2020, 142, 9158–9162

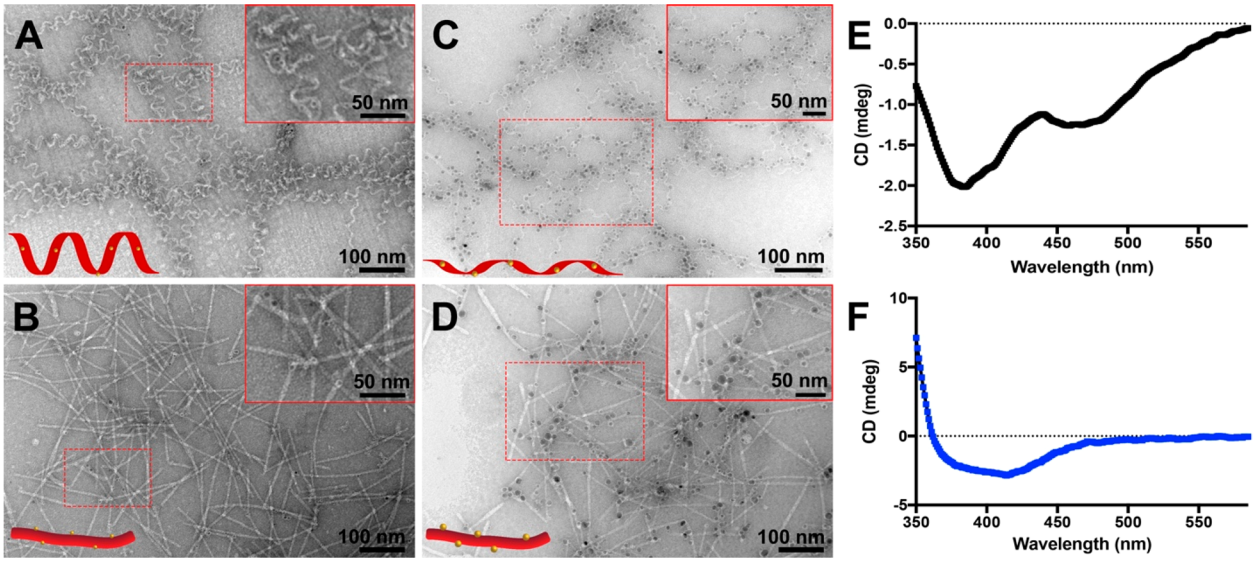

Figure 2. (A–D) TEM images of (A) AgSD/$\mathbf{K_SC'EK_S}$ nanohelices, (B) AgSD/$\mathbf{C'EK_SK_S}$ nanoribbons, (C) AgNP/$\mathbf{K_SC'EK_S}$ nanohelices, and (D) AgNP/$\mathbf{C'EK_SK_S}$ nanoribbons. Inserts in the top right corners of panels A–D show zoomed-in images of the areas outlined by the dashed red rectangles. (E and F) CD spectra of (E) AgNP/$\mathbf{K_SC'EK_S}$ nanohelices and (F) AgNP/$\mathbf{C'EK_SK_S}$ nanoribbons.

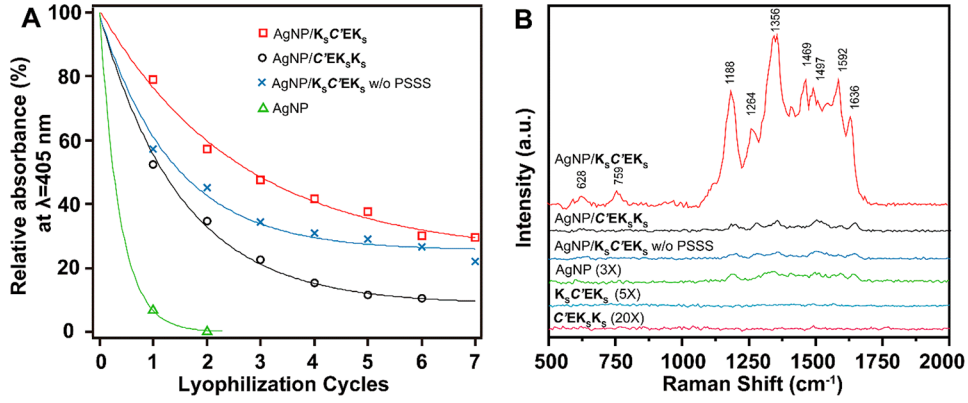

Figure 3. (A) Colloidal stability of all groups studied in the present work against lyophilization. Comparing the decay rates of the intensities of the LSPR absorbance peak corresponding to AgNPs ($\lambda_{LSPR} \approx 405$ nm) indicates the resistance of AgNPs to aggregation. The peak intensity prior to lyophilization serves as a reference for normalization (100% relative absorbance). Data were fitted with an exponential model (see Supporting Information for details). (B) SERS spectra of 10^{-4} M RhB collected on all AgNP/APA hybrids, pure AgNPs, and pure APAs. Spectra of control samples were intensified as indicated for better visualization.

presence of $\mathbf{K_SC'EK_S}$ nanohelices, the diameter of the AgSDs was 2.8 ± 0.5 nm (Figure 2A). After the second round of Ag growth, the diameter of the AgNPs increased to 7.6 ± 0.9 nm (Figure 2C). When $\mathbf{C'EK_SK_S}$ nanoribbons were used as the template under the same growth conditions, AgSDs and AgNPs formed with diameters of 2.9 ± 0.6 nm (Figure 2B) and 8 ± 1 nm (Figure 2D), respectively. Although the sizes of the AgSDs and the AgNPs were similar on both the nanohelices and the nanoribbons, the AgSDs and AgNPs in these two-dimensional conventional TEM images appeared to distribute mostly on the concave side of the curves and therefore within the $\mathbf{K_SC'EK_S}$ nanohelices (Figure 2A and 2C), while those templated by the $\mathbf{C'EK_SK_S}$ nanoribbons distributed at the edges of the nanoribbons (Figure 2B and 2D). We also prepared AgNP/$\mathbf{K_SC'EK_S}$ hybrids without PSSS, which as we noted above was vital for nanohelix formation. These AgSD and AgNP arrays had similar appearance and dimensions (2.6 ± 0.9 nm for AgSDs and 8 ± 1 nm for AgNPs) to the nanoribbon-forming AgNP/$\mathbf{C'EK_SK_S}$ hybrids. These results demonstrate that both APAs functioned as templates for AgNP growth, regulating the spatial arrangement of these nanoparticles.

CD spectroscopy allowed us to investigate the chirality of the resultant hybrids. The CD spectrum of AgNP/$\mathbf{K_SC'EK_S}$ displayed three negative peaks (Figure 2E), whereas that of AgNP/$\mathbf{C'EK_SK_S}$ exhibited only a broad negative peak (Figure 2F). For an achiral assembly of AgNPs, a flat CD spectrum would be expected, so these spectra confirmed that chirality was transferred from the APA nanoassemblies to these hybrid structures, similar to AgNPs templated by DNA.[13] In addition, the absorption beyond 470 nm was much stronger for AgNP/$\mathbf{K_SC'EK_S}$ than for AgNP/$\mathbf{C'EK_SK_S}$; this spectral feature may indicate a stronger interaction between AgNPs and $\mathbf{K_SC'EK_S}$ nanohelices than $\mathbf{C'EK_SK_S}$ nanoribbons.[36]

Next, we evaluated the stability of the AgNP/APA hybrids through multiple lyophilization cycles, as this property is critical for storage and practical applications. The stability was assessed by measuring the intensity of the localized surface

https://dx.doi.org/10.1021/jacs.0c03672
J. Am. Chem. Soc. 2020, 142, 9158–9162

plasmonic resonance (LSPR) absorption of the AgNPs at 405 nm, which reflects the concentration of dispersed AgNPs in solution. The absorbance of all hybrids and pure AgNPs of similar size decreased with each lyophilization cycle (Figures 3A and S9). Specifically, the absorbance of the helical AgNP/$\mathbf{K_SC'EK_S}$ hybrids decreased to 80% of its original value after one lyophilization cycle, while nanoribbon-forming AgNP/$\mathbf{C'EK_SK_S}$ hybrids decreased to 55%. Similarly, the absorption of AgNP/$\mathbf{K_SC'EK_S}$ nanoribbons prepared without PSSS decreased to 58% after one lyophilization cycle. The absorption of pure AgNPs (without any APA template) after one cycle decreased to 5% of its original value. Notably, all the hybrids could be rehydrated and resuspended after several cycles of lyophilization, while pure AgNPs could not. We conducted similar colloidal stability studies by adding increasing amounts of salt (PB) to these three types of AgNP/APA hybrids along with pure AgNPs (Figure S10). Results showed that all AgNP/APA hybrids tolerated salt better than pure AgNPs.

Finally, given the different spatial arrangements of AgNPs on the self-assembled APAs, we asked whether these hybrids could be used as substrates for SERS. Specifically, we investigated whether APA morphology in these AgNP/APA hybrids would affect SERS sensitivity. We selected rhodamine B (RhB) and 2,2′-bipyridine (Bpy) as model SERS analytes. Notably, for both analytes, the helical AgNP/$\mathbf{K_SC'EK_S}$ hybrids outperformed all other materials investigated. In the case of RhB, it enhanced the characteristic Raman bands to a much greater extent than the two nanoribbon-forming controls, AgNP/$\mathbf{C'EK_SK_S}$ and AgNP/$\mathbf{K_SC'EK_S}$ without PSSS (Figure 3B). Additional control systems including pure AgNPs (no APA template) as well as the APAs $\mathbf{K_SC'EK_S}$ and $\mathbf{C'EK_SK_S}$ without AgNPs were also investigated for comparison. The pure AgNPs displayed a weak SERS signal, while the APAs alone showed no discernible SERS signal. We also observed the same trend of SERS enhancement when Bpy was used as the analyte (Figure S11).

These results indicate that the spatial arrangement of AgNPs into the helical configuration provided by $\mathbf{K_SC'EK_S}$ is key for superior SERS enhancement over its nanoribbon-forming counterparts because the size and shape of the AgNPs investigated were the same. We hypothesize that AgNPs within the grooves of $\mathbf{K_SC'EK_S}$ nanohelices were better immobilized and provided a more favorable 3D arrangement for SERS than the AgNPs on the nanoribbons ($\mathbf{C'EK_SK_S}$ or $\mathbf{K_SC'EK_S}$ without PSSS). Compared to commonly used SERS substrates that are either plasmonic NPs grafted with ligands or lithographically patterned metal surfaces,[37−40] our constructs provide unique particle arrangements, require negligible energy input, possess high colloidal stability, and are dispersible in biological media.

In summary, we have reported a simple strategy to construct chiral AgNP hybrids from two APAs, $\mathbf{K_SC'EK_S}$ and $\mathbf{C'EK_SK_S}$, both of which initially assembled into nanoribbons with similar dimensions. However, when silver ions and PSSS were added, one of nanoribbons ($\mathbf{K_SC'EK_S}$) transformed into nanohelices. Both nanostructures served as effective templates for AgNP growth, and the resulting hybrids showed improved stability over pure AgNPs. We found that these hybrid materials were suitable as SERS substrates, with the nanohelix-forming hybrids exhibiting a superior signal enhancement driven by the unique spatial arrangement of AgNPs compared to their nanoribbon counterparts. This work highlights how small changes in molecular structure can dramatically alter plasmonic properties. We believe this strategy reveals novel ways to construct sophisticated peptide-based nanostructures for biomedical applications such as biomarker detection.

■ ASSOCIATED CONTENT

Supporting Information

The Supporting Information is available free of charge at https://pubs.acs.org/doi/10.1021/jacs.0c03672.

Detailed experimental section and additional characterization (ESI-MS, UV−vis, circular dichroism) (PDF)

■ AUTHOR INFORMATION

Corresponding Authors

Guoliang Liu − *Department of Chemistry and Macromolecules Innovation Institute, Virginia Tech, Blacksburg, Virginia 24061, United States;* orcid.org/0000-0002-6778-0625; Email: gliu1@vt.edu

John B. Matson − *Department of Chemistry and Macromolecules Innovation Institute, Virginia Tech, Blacksburg, Virginia 24061, United States;* orcid.org/0000-0001-7984-5396; Email: jbmatson@vt.edu

Authors

Yin Wang − *Department of Chemistry and Macromolecules Innovation Institute, Virginia Tech, Blacksburg, Virginia 24061, United States;* orcid.org/0000-0001-6729-7230

Xiaozhou Yang − *Department of Chemistry, Virginia Tech, Blacksburg, Virginia 24061, United States*

Tianyu Liu − *Department of Chemistry, Virginia Tech, Blacksburg, Virginia 24061, United States;* orcid.org/0000-0002-8716-749X

Zhao Li − *Department of Chemistry and Macromolecules Innovation Institute, Virginia Tech, Blacksburg, Virginia 24061, United States*

David Leskauskas − *Department of Chemistry, Virginia Tech, Blacksburg, Virginia 24061, United States*

Complete contact information is available at: https://pubs.acs.org/10.1021/jacs.0c03672

Notes

The authors declare no competing financial interest.

■ ACKNOWLEDGMENTS

This work was supported by the Virginia Tech Dean's Discovery Fund, the National Science Foundation (DMR-1454754 and DMR-1752611), and the National Institutes of Health (R01GM123508). We thank Prof. Tijana Grove (Virginia Tech) and her students for experimental assistance, Prof. Peter Vikesland for helpful discussions, and Samantha J. Scannelli and Kearsley M. Dillon for careful readings of the manuscript. The authors acknowledge use of facilities within the Nanoscale Characterization and Fabrication Laboratory at Virginia Tech.

■ REFERENCES

(1) Kundu, S. Formation of self-assembled Ag nanoparticles on DNA chains with enhanced catalytic activity. *Phys. Chem. Chem. Phys.* **2013**, *15*, 14107−14119.

(2) Singh, P.; Lamanna, G.; Menard-Moyon, C.; Toma, F. M.; Magnano, E.; Bondino, F.; Prato, M.; Verma, S.; Bianco, A. Formation of efficient catalytic silver nanoparticles on carbon nanotubes by

adenine functionalization. *Angew. Chem., Int. Ed.* **2011**, *50*, 9893−9897.
(3) Yao, J.; Yang, M.; Duan, Y. X. Chemistry, biology, and medicine of fluorescent nanomaterials and related systems: New insights into biosensing, bioimaging, genomics, diagnostics, and therapy. *Chem. Rev.* **2014**, *114*, 6130−6178.
(4) Zeng, S. W.; Baillargeat, D.; Ho, H. P.; Yong, K. T. Nanomaterials enhanced surface plasmon resonance for biological and chemical sensing applications. *Chem. Soc. Rev.* **2014**, *43*, 3426−3452.
(5) Rizzello, L.; Pompa, P. P. Nanosilver-based antibacterial drugs and devices: Mechanisms, methodological drawbacks, and guidelines. *Chem. Soc. Rev.* **2014**, *43*, 1501−1518.
(6) Rai, M.; Yadav, A.; Gade, A. Silver nanoparticles as a new generation of antimicrobials. *Biotechnol. Adv.* **2009**, *27*, 76−83.
(7) Wiley, B.; Sun, Y. G.; Xia, Y. N. Synthesis of silver nanostructures with controlled shapes and properties. *Acc. Chem. Res.* **2007**, *40*, 1067−1076.
(8) Nie, Z. H.; Petukhova, A.; Kumacheva, E. Properties and emerging applications of self-assembled structures made from inorganic nanoparticles. *Nat. Nanotechnol.* **2010**, *5*, 15−25.
(9) Huang, F.; Gao, Y.; Zhang, Y. M.; Cheng, T. J.; Ou, H. L.; Yang, L. J.; Liu, J. J.; Shi, L. Q.; Liu, J. F. Silver-decorated polymeric micelles combined with curcumin for enhanced antibacterial activity. *ACS Appl. Mater. Interfaces* **2017**, *9*, 16880−16889.
(10) Hoque, J.; Yadav, V.; Prakash, R. G.; Sanyal, K.; Haldar, J. Dual-function polymer-silver nanocomposites for rapid killing of microbes and inhibiting biofilms. *ACS Biomater. Sci. Eng.* **2019**, *5*, 81−91.
(11) Li, R. C.; Wang, H.; Song, Y.; Lin, Y. N.; Dong, M.; Shen, Y. D.; Khan, S.; Zhang, S. Y.; Fan, J. W.; Zhang, F. W.; Su, L.; Wooley, K. L. *In situ* production of Ag/polymer asymmetric nanoparticles via a powerful light-driven technique. *J. Am. Chem. Soc.* **2019**, *141*, 19542−19545.
(12) Pal, S.; Sharma, J.; Yan, H.; Liu, Y. Stable silver nanoparticle-DNA conjugates for directed self-assembly of core-satellite silver-gold nanoclusters. *Chem. Commun.* **2009**, 6059−6061.
(13) Shemer, G.; Krichevski, O.; Markovich, G.; Molotsky, T.; Lubitz, I.; Kotlyar, A. B. Chirality of silver nanoparticles synthesized on DNA. *J. Am. Chem. Soc.* **2006**, *128*, 11006−11007.
(14) Vasylevskyi, S. I.; Kracht, S.; Corcosa, P.; Fromm, K. M.; Giese, B.; Fueg, M. Formation of silver nanoparticles by electron transfer in peptides and c-cytochromes. *Angew. Chem., Int. Ed.* **2017**, *56*, 5926−5930.
(15) Kalakonda, P.; Banne, S. Synthesis and optical properties of highly stabilized peptide-coated silver nanoparticles. *Plasmonics* **2018**, *13*, 1265−1269.
(16) Pazos, E.; Sleep, E.; Perez, C. M. R.; Lee, S. S.; Tantakitti, F.; Stupp, S. I. Nucleation and growth of ordered arrays of silver nanoparticles on peptide nanofibers: Hybrid nanostructures with antimicrobial properties. *J. Am. Chem. Soc.* **2016**, *138*, 5507−5510.
(17) Lin, Y. Y.; Pashuck, E. T.; Thomas, M. R.; Amdursky, N.; Wang, S. T.; Chow, L. W.; Stevens, M. M. Plasmonic chirality imprinting on nucleobase-displaying supramolecular nanohelices by metal-nucleobase recognition. *Angew. Chem., Int. Ed.* **2017**, *56*, 2361−2365.
(18) Diez, I.; Hahn, H.; Ikkala, O.; Borner, H. G.; Ras, R. H. A. Controlled growth of silver nanoparticle arrays guided by a self-assembled polymer-peptide conjugate. *Soft Matter* **2010**, *6*, 3160−3162.
(19) Reithofer, M. R.; Lakshmanan, A.; Ping, A. T. K.; Chin, J. M.; Hauser, C. A. E. *In situ* synthesis of size-controlled, stable silver nanoparticles within ultrashort peptide hydrogels and their anti-bacterial properties. *Biomaterials* **2014**, *35*, 7535−7542.
(20) Matson, J. B.; Stupp, S. I. Self-assembling peptide scaffolds for regenerative medicine. *Chem. Commun.* **2012**, *48*, 26−33.
(21) Wang, Y.; Cheetham, A. G.; Angacian, G.; Su, H.; Xie, L. S.; Cui, H. G. Peptide-drug conjugates as effective prodrug strategies for targeted delivery. *Adv. Drug Delivery Rev.* **2017**, *110*, 112−126.
(22) Fleming, S.; Ulijn, R. V. Design of nanostructures based on aromatic peptide amphiphiles. *Chem. Soc. Rev.* **2014**, *43*, 8150−8177.
(23) Worthington, P.; Langhans, S.; Pochan, D. Beta-hairpin peptide hydrogels for package delivery. *Adv. Drug Delivery Rev.* **2017**, *110*, 127−136.
(24) Hamley, I. W. Small bioactive peptides for biomaterials design and therapeutics. *Chem. Rev.* **2017**, *117*, 14015−14041.
(25) Wang, Y.; Kaur, K.; Scannelli, S. J.; Bitton, R.; Matson, J. B. Self-assembled nanostructures regulate H_2S release from constitutionally isomeric peptides. *J. Am. Chem. Soc.* **2018**, *140*, 14945−14951.
(26) Foster, J. C.; Powell, C. R.; Radzinski, S. C.; Matson, J. B. *S*-Aroylthiooximes: A facile route to hydrogen sulfide releasing compounds with structure-dependent release kinetics. *Org. Lett.* **2014**, *16*, 1558−1561.
(27) Wang, Y.; Matson, J. B. Supramolecular nanostructures with tunable donor loading for controlled H_2S release. *ACS Appl. Bio Mater.* **2019**, *2*, 5093−5098.
(28) Qian, Y.; Kaur, K.; Foster, J. C.; Matson, J. B. Supramolecular tuning of H_2S release from aromatic peptide amphiphile gels: Effect of core unit substituents. *Biomacromolecules* **2019**, *20*, 1077−1086.
(29) Kaur, K.; Wang, Y.; Matson, J. B. Linker-regulated H_2S release from aromatic peptide amphiphile hydrogels. *Biomacromolecules* **2020**, *21*, 1171−1178.
(30) Longchamp, A.; Kaur, K.; Macabrey, D.; Dubuis, C.; Corpataux, J. M.; Deglise, S.; Matson, J. B.; Allagnat, F. Hydrogen sulfide-releasing peptide hydrogel limits the development of intimal hyperplasia in human vein segments. *Acta Biomater.* **2019**, *97*, 374−384.
(31) Carter, J. M.; Qian, Y.; Foster, J. C.; Matson, J. B. Peptide-based hydrogen sulphide-releasing gels. *Chem. Commun.* **2015**, *51*, 13131−13134.
(32) Khan, A. U.; Zhou, Z. P.; Krause, J.; Liu, G. L. Poly(vinylpyrrolidone)-free multistep synthesis of silver nanoplates with plasmon resonance in the near infrared range. *Small* **2017**, *13*, 1701715.
(33) Gibb, B. C. Hofmeister's curse. *Nat. Chem.* **2019**, *11*, 963−965.
(34) Cui, H. G.; Cheetham, A. G.; Pashuck, E. T.; Stupp, S. I. Amino acid sequence in constitutionally isomeric tetrapeptide amphiphiles dictates architecture of one-dimensional nanostructures. *J. Am. Chem. Soc.* **2014**, *136*, 12461−12468.
(35) Khan, A. U.; Zhao, S. Q.; Liu, G. L. Key parameter controlling the sensitivity of plasmonic metal nanoparticles: Aspect ratio. *J. Phys. Chem. C* **2016**, *120*, 19353−19364.
(36) Maoz, B. M.; van der Weegen, R.; Fan, Z. Y.; Govorov, A. O.; Ellestad, G.; Berova, N.; Meijer, E. W.; Markovich, G. Plasmonic chiroptical response of silver nanoparticles interacting with chiral supramolecular assemblies. *J. Am. Chem. Soc.* **2012**, *134*, 17807−17813.
(37) Wang, H.; Levin, C. S.; Halas, N. J. Nanosphere arrays with controlled sub-10-nm gaps as surface-enhanced Raman spectroscopy substrates. *J. Am. Chem. Soc.* **2005**, *127*, 14992−14993.
(38) Guerrini, L.; Graham, D. Molecularly-mediated assemblies of plasmonic nanoparticles for Surface-Enhanced Raman Spectroscopy applications. *Chem. Soc. Rev.* **2012**, *41*, 7085−7107.
(39) Sharma, B.; Frontiera, R. R.; Henry, A. I.; Ringe, E.; Van Duyne, R. P. SERS: Materials, applications, and the future. *Mater. Today* **2012**, *15*, 16−25.
(40) Tessier, P.; Velev, O. D.; Kalambur, A. T.; Lenhoff, A. M.; Rabolt, J. F.; Kaler, E. W. Structured metallic films for optical and spectroscopic applications via colloidal crystal templating. *Adv. Mater.* **2001**, *13*, 396−400.

https://dx.doi.org/10.1021/jacs.0c03672
J. Am. Chem. Soc. 2020, 142, 9158−9162